Deformation of soap films pushed through tubes at high velocity

Benjamin Dollet, Isabelle Cantat

Deformation of soap films pushed through tubes at high velocity

Benjamin Dollet[1] **and Isabelle Cantat**[1]

[1] Institut de Physique de Rennes, UMR 6251 CNRS/Université de Rennes 1, Campus Beaulieu, Bâtiment 11A, 35042 Rennes Cedex, France.

(Received 1 February 2010)

The behaviour of soap films pushed through tubes at large velocities, up to several m/s, is investigated. The film shape deviates from its equilibrium configuration perpendicular to the walls and gets curved downstream. A simple model relates the radius of curvature of the film to the friction in the lubrication films touching the wall, and the scaling of Bretherton (1961) holds up to surprisingly high velocities, at which the capillary and Weber numbers are no longer small parameters. The tube geometry is varied and accounted for through the notion of hydraulic diametre. A limit of stability of the film, beyond which the films burst or evolve unsteadily, is predicted, and captures quantitatively the observations. The new questions raised by our results on the dissipation in soap films are discussed, especially the role of Plateau borders and inertial effects.

1. Introduction

Aqueous foams are widely used in industry, in areas as diverse as ore flotation, oil extraction, food and pharmaceutical production and blast noise reduction, to cite a few. Many foam flows of practical interest are dominated by viscous friction because of high velocity gradients, either in bulk, or localised close to confining boundaries. For instance,

foams in porous media, used for enhanced oil recovery (Hirasaki & Lawson 1985) and soil remediation (Chowdiah *et al.* 1998), often flow through narrow gaps as a train of soap films, in contact with the confining walls through Plateau borders (PBs) where viscous dissipation takes place and dictates the foam flow properties (Rossen & Gauglitz 1990; Kornev *et al.* 1999). The influence of confinement is also paramount in microfluidics, where foams are used in lab-on-a-chip applications (see Marmottant & Raven (2009) for a review).

Foam flows dominated by viscous friction are also of fundamental interest: foam rheology has received a considerable attention in recent years (Höhler & Cohen-Addad 2005), but mostly at velocities small enough for the foam to remain in equilibrium configurations, i.e. for structural equilibrium rules to apply. However, deviations from these equilibrium rules have been recently evidenced (Drenckhan *et al.* 2005; Besson *et al.* 2008), due to bubble/bubble or bubble/wall viscous friction. This calls for more studies of foam rheology at high velocity gradients, where the structure is brought out of equilibrium because of a high viscous resistance.

In this paper, we study the most elementary experiment of high-velocity foam rheology in confined media: the fast flow of an isolated soap film pushed through a tube of constant section. We especially quantify over a full range its shape deviation from the simple equilibrium configuration, perpendicular to the confining walls. We extract a precise experimental criterion for its rupture in terms of critical velocity.

2. Materials and methods

A glass tube was connected through flexible plastic tubes to a pressurised nitrogen bottle, which supplies nitrogen through an electronic flow-rate controller (Brooks) (Fig. 1). We have used three circular glass tubes, of inner diameters 3.6, 5.9 and 8.8 mm, and a

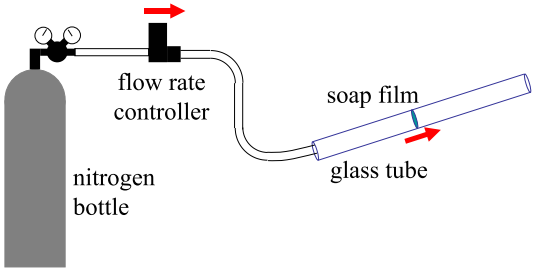

FIGURE 1. Sketch of the experimental setup.

square one, of side 10.0 mm with rounded edges of radius of curvature lower than 1 mm. The tube is tilted upwards with an angle of about 20° with respect to the horizontal, so that the plastic tube to which it is connected is at lower level and can be used as soap reservoir. Soap solution is injected by a syringe, directly through the open end of the glass tube. When turned on, the gas flows into this reservoir, and creates soap films which are subsequently pushed through the glass tube. Transient effects were also investigated using films prepared first at low velocity, and then accelerated (Sec. 4.2). When starting an experiment, we waited for the solution to wet entirely the glass walls, because of the first soap injections and films. The wetting film remains intact during the whole experiment: the signature of dewetting would be the nucleation and growth of dry patches and an irregular behaviour of the films that was never observed.

The soap solution is a solution of SDS (Sigma-Aldrich) dissolved in a mixture of ultrapure water (Millipore) and of 10% wt glycerol (Sigma-Aldrich). The concentration of SDS is 10 g/l, above the critical micellar concentration (cmc) of 2.3 g/l. Its bulk viscosity, measured in a Couette rheometer (Anton Paar) is $\eta = 1.2$ mPa s. Its surface static and dynamic properties were measured with a tensiometer (Teclis) by the rising bubble and oscillating bubble method; the surface tension is $\sigma = 36.8 \pm 0.3$ mN/m and the surface modulus E_S, defined as in Denkov *et al.* (2005), was below the noise level of 1 mN/m at frequency 0.2 Hz. All solutions were used within a day from fabrication.

The motion of a soap film is recorded with a high-speed camera (Photron APX-RS) in the central zone of the glass tube, to avoid end effects. The main results, presented in Sec. 4.1, have been obtained with a 2 cm long field of view (measured along the tube axis). We checked that no significant variations of shape and velocity occur along this trajectory: hence, the data in Sec. 4.1 concern steady film motions. Additionnal experiments, discussed in Sec. 4.2, have been made on unsteady film motions, with a 15 cm long field of view to investigate the long range stability of the films, especially for the highest velocity values. Exemples of imaged soap films are displayed in Figs. 2 (circular tube) and 3 (square tube). From each movie, we plot as a spatiotemporal diagram (z,t), with z the streamwise axis and t the time, the evolution of the gray levels along the tube centreline (Fig. 4a). The soap film appears as a dark band, which slope α yields the film velocity v: $v = \mathrm{d}z/\mathrm{d}t = \cot\alpha$. The slope can be extracted with an accuracy better than $\delta\alpha = 0.1°$, which gives the uncertainty on v: $\delta v = \delta\alpha/\sin^2\alpha$.

Above a given velocity of order 40 cm/s, the soap film shows a significant curvature pointing downstream (Figs. 2b,c and 4b). To measure this curvature, we have performed the following home-made contour detection procedure. First, we have thresholded and binarised the images (Fig. 4c), then we have extracted the coordinates (ξ, z) of the points located on the curved profile ($\xi = 0$ at the centre of the tube). This set of coordinates was then fitted to the polynomial approximation of degree four of a circle of radius R: $-z = (\xi-\xi_0)^2/2R + (\xi-\xi_0)^4/8R^3$ and we extract R as the best fit parameter (Fig. 4d). The offset ξ_0 is required because, in some experiments, the soap film is not symmetric, as in Fig. 2b where the top part of the film lags behind. All this procedure assumes a constant curvature; we confirmed that this was a realistic assumption by checking the close agreement between the whole experimental trace and the best fit, which also gives a small relative uncertainty on the fitting parameter R (this uncertainty is represented

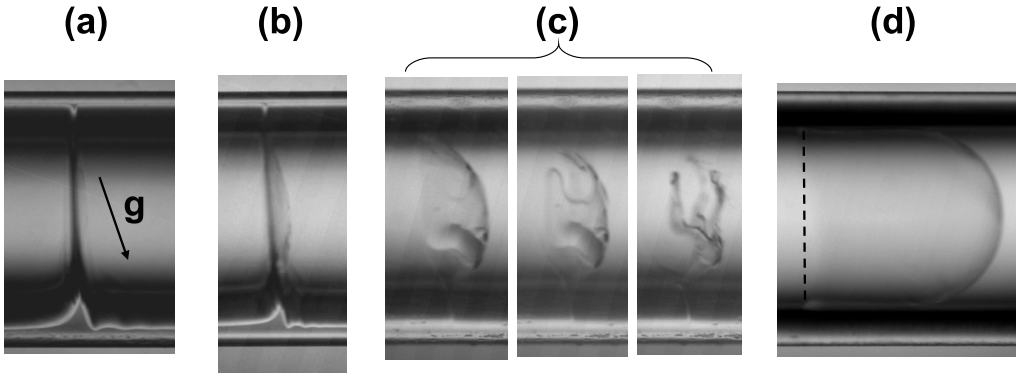

FIGURE 2. Snapshots of soap films pushed from left to right through a tube of outer diameter 9.0 mm, at velocities (a) 0.37, (b) 0.64, (c) 1.81 and (d) 2.47 m/s. Films (a) and (b) were observed to be stable, and films (c) and (d) displayed an unsteady behaviour: film (c) broke down as shown in the three consecutive displayed frames (interframe 0.33 ms), whereas film (d) tends to detach from its Plateau border (PB) through a long cylindrical neck, which eventually leads to film bursting or pinch-off of a bubble (see Sec. 4.2). Notice the top-bottom asymmetry of the PB, due to drainage [the direction of gravity is indicated in (a)], and, in (a) and (b), the damped oscillations of the wetting film ahead of the PB in contrast with the monotonous profile of the wetting film at the rear of the PB.

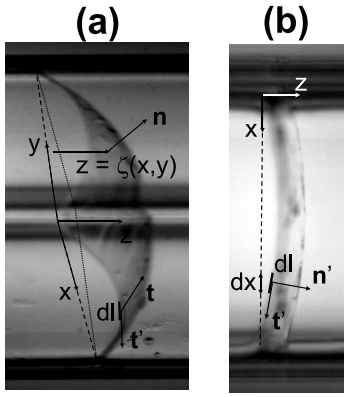

FIGURE 3. Snapshots of soap films pushed from left to right through a square tube of side 10.0 mm, (a) in tilted view, to get an impression of the whole shape, and (b) facing one of the four sides: the front part of the shape is the trace of the central part of the film, and the back part is the PB in contact with the imaged side. This is the view used to measure the radius of curvature of the film. The superimposed notations are used in Sec. 3.

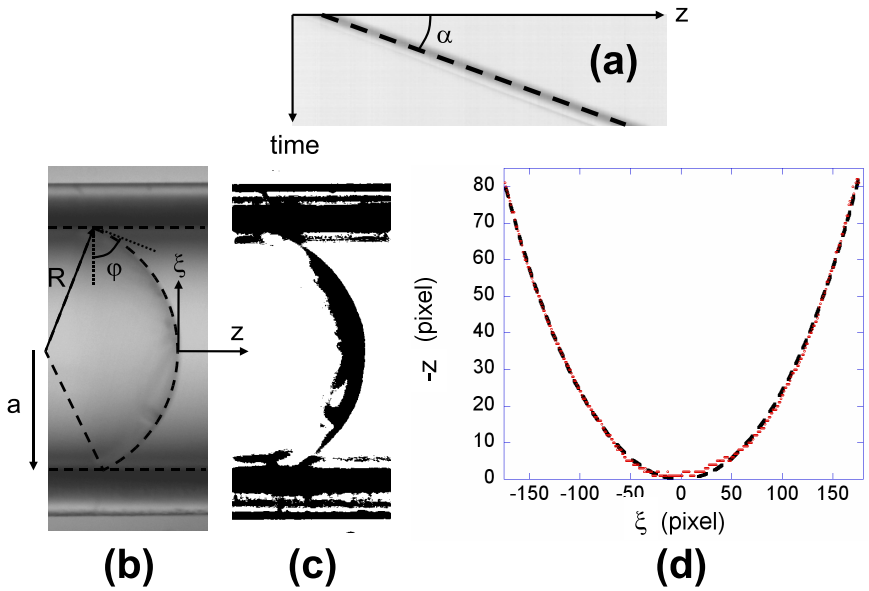

FIGURE 4. (a) Example of a spatiotemporal diagram. The film is represented by a straight dark band. To measure the film curvature, the raw image (b) is binarised (c), and (d) the coordinates of the film contour are extracted (dotted curve) and fitted by a circle (dashed curve), also superimposed in (b) with various notations used in the text.

by the vertical error bars in Fig. 5). Notice that the film curvature is not measurable at lower velocities, because the curved profile is hidden by the thicker trace of the PB (Fig. 2a).

3. Theory

3.1. *Film deformation*

We consider the steady motion of a soap film pushed at imposed velocity v through a cylindrical tube of arbitrary shape, with a perimeter $\mathcal{P}$ and a cross-section $\mathcal{S}$. The film displays a curvature H because of the pressure drop ΔP associated to its motion, due to the viscous friction in the liquid. After Laplace law, the two latter quantities are related through: $\Delta P = 2\sigma H$, accounting for the fact that the soap films is bounded by two gas/liquid interfaces. Hence, if the pressure on both sides of the film are equilibrated, the

film has a constant curvature. Here, we assume that the surface tension is constant in the transverse soap film (it needs not be in the PB; see Sec. 5.2). Following the assumption of Cantat *et al.* (2004), we assume that the friction force of an elementary length $\mathrm{d}\ell$ of PB, of normal unit vector pointing downstream $\mathbf{n}'$ (Fig. 3), is proportional to its projected length across the tube, $\mathrm{d}\ell\ \mathbf{n}' \cdot \mathbf{e}_z$, and to the friction force $f(v)$ per unit PB length; therefore, the total friction force experienced by the soap film is $\mathcal{P}f(v)$. Hence, the steady motion of the soap film obeys the equation: $2\sigma\mathcal{S}H = \mathcal{P}f(v)$.

In our experiments, close to the centre of the tubes, the film shows a constant radius of curvature R; therefore, $H = 2/R$. Let further $b = 4\mathcal{S}/\mathcal{P}$ be the hydraulic diametre of the tube; for a circular tube of radius a, $b = 2a$, and for a square tube of side c, $b = c$. Thus, we have the simple prediction that R/b should be independent from the tube geometry:

$$\frac{R}{b} = \frac{\sigma}{f(v)}. \tag{3.1}$$

3.2. *Limit of steady film deformation*

The above discussion assumed the existence of a steady shape of the soap film into motion. This clearly fails at high velocity, because the curvature of the film becomes too high for the film to meet the tube.

This idea is easy to quantify for a circular tube of radius a. A transverse film in steady motion meets then the wall tube with a constant angle φ, obeying $\sin\varphi = a/R$ (Fig. 4b), and $f(v) = 2\sigma\sin\varphi$ after (3.1). Hence, the minimal radius of curvature is simply:

$$R_{\min}^{\text{circle}} = a = \frac{b}{2}, \tag{3.2}$$

and $f(v)$ cannot exceed 2σ.

For a square tube, the film shape should be of constant curvature and compatible with the local viscous friction on the boundary. Let $z = \zeta(x, y)$ be the equation of the film in the square domain $0 \leq x, y \leq a$. We consider an elementary portion of a PB in contact

with a wall, say at $y = 0$, of length $\mathrm{d}\ell$ and of projected length dx (Fig. 3). This portion of PB meets the upstream and downstream wetting films, which tensions cancel out, and the transverse film, which two gas/liquid interfaces exert a tension in its locally tangential direction $\mathbf{t}$ along the length $\mathrm{d}\ell$. Furthermore, it experiences a viscous force $-f(v)\ \mathrm{d}x\ \mathbf{e}_z$. Hence, the force balance along $\mathbf{e}_z$ on the portion of PB writes: $-f_v \mathrm{d}x + 2\sigma\ \mathrm{d}\ell\ \mathbf{t}\cdot\mathbf{e}_z = 0$. Moreover, $\mathbf{t} = \mathbf{n}\wedge\mathbf{t}'$, where $\mathbf{n} = (-\zeta_x\mathbf{e}_x - \zeta_y\mathbf{e}_y + \mathbf{e}_z)/\sqrt{1+\zeta_x^2+\zeta_y^2}$ is the normal unit vector of the transverse film, and $\mathbf{t}' = (\mathbf{e}_x + \zeta_x\mathbf{e}_z)/\sqrt{1+\zeta_x^2}$ is the tangential unit vector along the portion of PB. Hence, $\mathbf{t}\cdot\mathbf{e}_z = \zeta_y/\sqrt{(1+\zeta_x^2)(1+\zeta_x^2+\zeta_y^2)}$. Given that $\mathrm{d}x/\mathrm{d}\ell = 1/\sqrt{1+\zeta_x^2}$, the force balance gives the condition:

$$\frac{f(v)}{2\sigma} = \frac{\zeta_y}{\sqrt{1+\zeta_x^2+\zeta_y^2}} = \cos\gamma, \tag{3.3}$$

which is analogous to a capillary surface meeting a wall at prescribed contact angle $\gamma = \pi/2 - \varphi$, studied by Concus & Finn (1969). They predicted that in a wedge of interior angle 2δ, there exists no bounded surface if $\gamma + \delta < \pi/2$. In our case, the square tube has four corners with an angle $\delta = \pi/4$, hence the condition of existence of a shape of a transverse film in steady motion writes simply: $\varphi \leq \pi/4$ or, after (3.3), $f(v)/\sigma \leq \sqrt{2}$. Hence, after (3.1), the minimal radius of curvature is:

$$R_{\min}^{\mathrm{square}} = \frac{c}{\sqrt{2}} = \frac{b}{\sqrt{2}}. \tag{3.4}$$

When the friction law $f(v)$ is known, inserting $R_{\min}$ in (3.1) yields a prediction of the maximal velocity of a stable soap film.

3.3. *Friction law*

Several investigations have studied the viscous friction associated to the motion of a soap film. In a seminal paper, Bretherton (1961) has proposed a theoretical expression for the friction associated to the motion of an infinitely long bubble in a tube, in the limit where inertia is negligible with respect to viscous and capillary effects, and where

the capillary number $\mathrm{Ca} = \eta v/\sigma$, comparing viscous and capillary effects, is small. In that case, viscous friction comes from the transition zone matching the flat wetting film between the bubble and the wall, and the bubble tip. The length of the transition zone, and the thickness of the wetting film h_∞, are slaved to the radius of the bubble tip, i. e. the tube radius, but this cancels out in the expression of $f(v)$:

$$f(v) = 4.70\beta\sigma\mathrm{Ca}^{2/3}, \tag{3.5}$$

The factor β depends on the boundary condition at the gas/liquid interface: for a free shear boundary condition (mobile interfaces), $\beta = 1$, whereas for a no-slip boundary condition (rigid interfaces), $\beta = 2^{1/3} \simeq 1.26$ (Appendix A). Hirasaki & Lawson (1985) later extended this result to the case of soap films, showing that the relevant length becomes the PB radius, although this does not alter the expression of $f(v)$. This idea was also used by Denkov *et al.* (2005) to predict the viscous dissipation associated to the flow of foams against a wall. Finally, combining (3.1) and (3.5), we get the prediction for the radius of curvature of the film:

$$R = \frac{b}{4.70\beta\mathrm{Ca}^{2/3}}. \tag{3.6}$$

We will compare our data to this formula in Sec. 4, before discussing its underlying limitations in Sec. 5, notably the possible role of the PB size and of inertial effects.

4. Experiments

4.1. *Film deformation*

We first plot for each circular tube R as a function on v, and we fit the data by a power law (inset of Fig. 5). We obtain exponents of -0.64 ± 0.08, -0.71 ± 0.04 and -0.71 ± 0.04 for tubes of respective radius 3.6, 5.9 and 8.8 mm, all compatible with $-2/3$. Next, fitting each series by a law $A/v^{2/3}$, and plotting the best fit parameter A as a function of a for

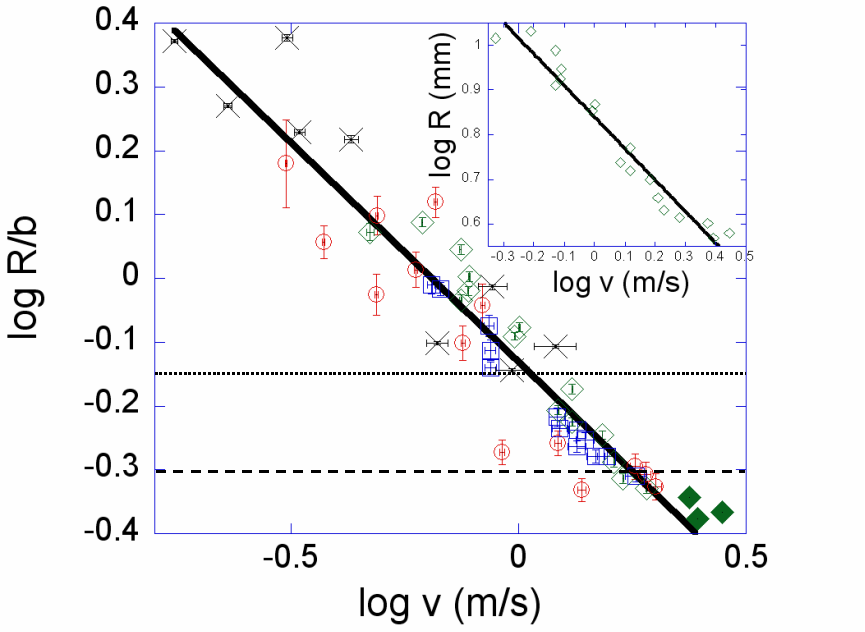

FIGURE 5. Plot of $\log R/b$ as a function of $\log v$ (expressed in m/s), for circular tubes of inner diameters 3.6 (○), 5.9 (□) and 8.8 mm (◊), and for the square tube of side 10.0 mm (×). The three points with the symbol ♦ were obtained in unsteady situations, see Sec. 4.2. The plain line represents the best linear fit through all data; its equation is $\log R/a = (-0.69 \pm 0.03) \log v - 0.131 \pm 0.008$. The dashed (dotted) line represents the theoretical limit of stability for soap films in circular (square) tubes. Inset: plot of $\log R$ (in mm) as a function of $\log v$, and its best linear fit, for the tube of diameter 8.8 mm.

the three tubes, we have checked that the data follow a linear law $A \propto a$ within 6% (data not shown). Hence, we can plot $R/2a$ as a function of v for all tubes (Fig. 5). The data collapse on a single curve, which best fit by a power law yields an exponent -0.65 ± 0.04. Therefore, the scaling $R \propto a/v^{2/3}$ predicted by (3.6) is experimentally verified, up to a velocity of 2.0 m/s, corresponding to a capillary number of 0.07.

Although somewhat more dispersed, the data for the square tube also follow a power

law with an exponent -0.67 ± 0.10 compatible with $-2/3$. According to Eq. (3.1), we rescale R by the square side c, and we plot R/c as a function of v in the same plot as the data for circular tubes (Fig. 5). All data collapse on the same master curve, showing that the hydraulic diameter is indeed the relevant geometrical length to compare tubes of different cross-sectional shapes. This master curve is a power law of exponent -0.69 ± 0.03, again compatible with an exponent $-2/3$.

Concerning the prefactor, the best fit of the data with a power law of exponent $-2/3$ gives $Rv^{2/3}/b = 0.74 \pm 0.02$ m$^{2/3}$, whereas inserting the measured solution properties in the prediction (3.6) gives $Rv^{2/3}/b = 2.08$ m$^{2/3}$ for $\beta = 1$ (mobile interfaces), and 1.66 m$^{2/3}$ for $\beta = 2^{1/3}$ (rigid interfaces).

4.2. *Unsteady behaviour and rupture of the soap films*

We now test the predictions of the minimal radius of curvature given by (3.2) and (3.4). The agreement with the most curved films that we were able to detect is excellent, within 2% for the square and 6% for the circular tubes (Fig. 5). No steady films have been recorded at higher velocity: they broke before entering the camera field of view.

To go beyond the limit of stability, we produced films at low velocity and accelerated them afterwards, typically 10 cm before they enter the field of view. With this procedure, when the gas flux is suddenly increased, the film is accelerated faster than the PBs, thus becomes much drier. Many films burst during this transient stage (Fig. 2c), but not all. With this procedure, few points have been obtained above the theoretical velocity limit on Fig. 5. They are still compatible with the friction law curve and their radius of curvature are then smaller than the theoretical predictions. As depicted on Fig. 2d, a long cylindrical neck is then present at the rear of the film. In order to evaluate the stability of these surprising shapes, we recorded images with a larger field of view (15 cm). These shape appeared to be unsteady. Several scenarii have been observed: breakage after few

centimeters; evolution towards the half sphere when the velocity is very close to the critical velocity; pinch-off of the neck into a separate bubble in some cases, that does not touch the wall anymore.

In contrast, we also checked that the shape recorded at velocity below the critical velocity does not change during the 15 cm long trajectory.

5. Discussion

5.1. *The weak influence of the Plateau border size*

We have hitherto disregarded the role of the PB size, which does not appear in Eq. (3.6) with which our measurements have been interpreted. However, we have observed in many cases (e.g. Fig. 2b) that the soap films are not symmetric. The top part of the PB, which is also the driest because of drainage, lags often significantly behind the bottom part, hence experiences more friction.

To quantify this possible influence of the PB size, we have extracted for the experiments with the circular tube of diameter 5.9 mm the two angles, φ_{top} and $\varphi_{\mathrm{bottom}}$, with which the soap film meets the top and bottom part of the tube. This gives a ratio on the friction force per unit PB length: $f(v)_{\mathrm{top}}/f(v)_{\mathrm{bottom}} = \sin\varphi_{\mathrm{top}}/\sin\varphi_{\mathrm{bottom}}$. For all experiments but one, we have checked that $\log|f(v)_{\mathrm{top}}/f(v)_{\mathrm{bottom}}|$ remains below 0.1, which is the order of magnitude of the scatter of the data points with respect to the master curve in Fig. 5.

Therefore, the PB size is a correction to the main variation of the radius of curvature, with the velocity, that can be neglected in a first approach. In the absence of a theoretical prediction, it may be possible to include its role using empirical laws such as the one proposed by Raufaste *et al.* (2009).

5.2. *Boundary condition: rigid or mobile interfaces?*

SDS is known to be very mobile at an air/water interface and to exchange quickly with the solution bulk in case of area variation. Nevertheless, the expansion rate in our experiment scales like $v/\ell \sim v/r\mathrm{Ca}^{1/3}$, with ℓ the length of the transition domain, and reaches 10^5 s^{-1} for the highest velocities. At such a high rate, concentration gradients can appear, which effect is to impede surface area variations, through Marangoni stress. The boundary condition to be used is thus not obvious. A local conservation of the interface area, as used by Denkov *et al.* (2005) for finite size bubbles, imposes that the whole wetting film interface moves at the film velocity v and is thus unacceptable : in our geometry, the total interface area decreases downstream and increases upstream. In Appendix A, we allow the wetting film interface to move with the wall, as a rigid interface. The area variation is assumed to occur on larger length scale and smaller time scale in the moving film or in the PB interfaces and to be without influence on $f(v)$. The viscous force for a rigid interface is 1.26 times larger than for a mobile interface, but it is still lower than our experimental result.

5.3. *Contribution of the Plateau border to the viscous force*

In Bretherton's classical result, the friction force is localised in the transition zone between the wetting film and an external infinite reservoir. Here, on the contrary, the PB has a finite size r. Recirculations, with velocities larger than the film velocity have been observed in the PB, when tiny bubbles were trapped there; they have also been predicted in numerical simulations (Saugey *et al.* 2006). This induces extra velocity gradients, estimated in Appendix B, showing that the contribution of the PB to the viscous force should be of the same order than the contribution of the transition domains. We show that this additional contribution scales as the Bretherton term, which could explain why the scaling $f(v) \sim \sigma\mathrm{Ca}^{2/3}$ still holds in our experiments.

5.4. *Absence of inertial correction*

Inertial effects can be estimated using the Weber number $W = \rho v^2 r/\sigma$, with $r \sim 10^{-4}$ m the PB characteristic size and $\rho = 10^3$ kg/m^3 the solution density. For our velocity range, W varies between 0.04 and 25: inertial effects should then be visible and even dominant in that velocity range. The viscous force scaling in $\mathrm{Ca}^{2/3}$, signature of the visco-capillary regime, is therefore somewhat unexpected in this regime. Actually, the friction force scales as $f(v) \sim \eta \ell v/h_\infty$. Quéré & de Ryck (1998) have considered the deviations of h_∞ and ℓ from the visco-capillary scaling as inertia becomes significant, see Eq. (3.20) in their article. However, the scaling $\ell/h_\infty \sim \mathrm{Ca}^{-1/3}$ remains whatever the value of W. Hence, since inertia modifies ℓ and h_∞ likewise, the scaling $f(v) \sim \sigma \mathrm{Ca}^{2/3}$ is unaffected by the inertial corrections, as observed experimentally here.

6. Concluding remarks

Our results show that the limit of stability of soap films pushed through tubes obeys simple theoretical predictions, which match the experiments with an excellent precision. Once the friction law is known, this gives a quantitative criterion on the maximal velocity of a foam flow in a confined geometry.

Concerning the viscous friction between the soap film and the wall, the scaling proposed by Bretherton (1961) was shown to hold beyond its expected range of validity, at rather high capillary and Weber numbers. In the frame of the long-standing debate on the boundary condition and the role of surfactants (Ratulowski & Chang 1990; Shen *et al.* 2002; Denkov *et al.* 2005), this calls for further investigations on the viscous dissipation associated with the motion of bubbles, films and foams close to walls. In this context, we are currently studying the role of surface viscoelasticity on soap film and foam flows in confined geometries.

I. Cantat acknowledges a grant from the Institut Universitaire de France.

Appendix A. Friction law: mobile *versus* rigid interfaces

Here we compute the contribution to f of the two transition domains between the PB and the wetting film, upstream (top sign in the equations when the symbols $\pm$ or $\mp$ appear) and downstream (bottom sign in the equations). We use the frame of the steady film in which the wall moves at velocity v. Both contributions $f^{\pm}$ are determined independently and in both cases we orient the x axis towards the thin wetting film. The velocity v is thus positive for the upstream interface and negative for the downstream interface. The lubrication equation allows to determine the velocity field as a function of the interface profile $h(x)$: $u(x,y) = (\sigma/\eta)\left(\lambda h y - \frac{1}{2}y^2\right)\partial^3 h/\partial x^3 + v$, with $\lambda = 1$ if the tangential stress is vanishing at the interface and $\lambda = 1/2$ if the interface moves at the wall velocity v. The governing equation for the interface profile is, with $\mathrm{Ca} = \eta|v|/\sigma$ and $\beta = 2/(3\lambda - 1)$, $\pm 3\beta\mathrm{Ca}(h_\infty - h) = h^3\partial^3 h/\partial x^3$. Using the rescaling $h = Hh_\infty$ and $x = Xh_\infty/(3\beta\mathrm{Ca})^{1/3}$ with h_∞ the wetting film thickness we get $H'''H^3 = \pm(1-H)$, with boundary conditions $H(\infty) = 1$, $H'(\infty) = 0$ and $H''(\infty) = 0$, where the prime denotes derivation with respect to X. Finally, the contribution to the viscous force is given by $f^{\pm} = \eta\int_{-\infty}^{\infty}\partial u/\partial y(y=0)dx$ that can be expressed as a function of the unknown solution $H^{\pm}(X)$ and of the various parameters involved in the rescaling. We obtain:

$$f^{\pm} = \lambda\sigma(3\beta\mathrm{Ca})^{2/3}\int_{-\infty}^{\infty} H^{\pm\prime\prime\prime}H^{\pm}dX. \qquad (\mathrm{A}\,1)$$

Finally the contribution $f^{\pm}$ of the two transition domains verifies $f^{\pm}(\lambda)/f^{\pm}(1) = \lambda\beta^{2/3}$ which gives $f^{\pm}(\mathrm{rigid})/f^{\pm}(\mathrm{mobile}) = f^{\pm}(1/2)/f^{\pm}(1) = 2^{1/3} \simeq 1.26$. This ratio is twice smaller than the thickening factor $h_\infty(\mathrm{rigid})/h_\infty(\mathrm{mobile}) = 4^{2/3}$ shown by Ratulowski & Chang (1990) and Shen *et al.* (2002). Actually, the wetting film thickness is determined from the matching condition $1/r = \partial^2 h/\partial x^2(-\infty)$, which gives $h_\infty = RH''(-\infty)(3\beta\mathrm{Ca})^{2/3}$.

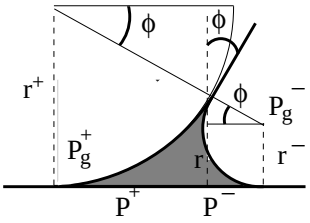

FIGURE 6. Sketch of a Plateau border.

Hence, h_∞ and f scale differently on λ and β, whence their different ratios between the mobile and rigid limits.

Appendix B. Contribution of the Plateau border to the friction

In addition to the contribution $f^{\pm}$ of the transition domains, the PB itself has a non-negligible contribution f^{PB} to the total viscous force per unit length. For a film flowing at velocity v in a tube of radius a, with a PB of typical size r, this contribution scales like $f^{PB} \sim \eta r v^{PB}/r \sim \eta v^{PB}$.

v^{PB} can either be governed by the wall motion, which implies $v^{PB} \sim v$, or by a pressure gradient due to the fore-aft asymmetry of the PB (Fig. 6), which implies $v^{PB} \sim (P^+ - P^-)r/\eta$. We compare both terms hereafter. The pressures are determined from the geometrical constraints governing the PB shape (see Fig. 6). Using the Laplace laws $P_g^{\pm} - P^{\pm} = \sigma/r^{\pm}$, $P_g^+ - P_g^- = 4\sigma \sin\phi/a$ and the geometrical relation $r^{\pm}(1 \mp \sin\phi) = r$, we get $P^+ - P^- \sim (P_g^+ - P_g^-)(1 + a/2r) \sim a(P_g^+ - P_g^-)/2r$. With $f = a(P_g^+ - P_g^-)/2$ we get finally $f^{PB}/f \sim 1$. The dissipation in the PB is thus not negligible in comparison with that in the transition region, and has the same scaling. From $f^{PB} \sim \eta v^{PB}$ we deduce $\mathrm{Ca}^{PB} \sim \mathrm{Ca}^{2/3}$, or $v^{PB}/v \sim \mathrm{Ca}^{-1/3} > 1$. The velocity in the PB is thus mainly governed by pressure effects and not only by the boundary velocity.

REFERENCES

Besson, S., Debrégeas, G., Cohen-Addad, S. & Höhler, R. 2008 Dissipation in a sheared foam: From bubble adhesion to foam rheology. *Phys. Rev. Lett.* **101**, 214504.

Bretherton, F. P. 1961 The motion of long bubbles in tubes. *J. Fluid Mech.* **10**, 166–188.

Cantat, I., Kern, N. & Delannay, R. 2004 Dissipation in foam flowing through narrow channels. *Europhys. Lett.* **65**, 726–732.

Chowdiah, P., Misra, B. R., Kilbane, J. J., Srivastava, V. J. & Hayes, T. D. 1998 Foam propagation through soils for enhanced in-situ remediation. *J. Hazardous Materials* **62**, 265–.

Concus, P. & Finn, R. 1969 On the behavior of a capillary surface in a wedge. *Proc. Natl. Acad. Sci.* **63**, 292–299.

Denkov, N. D., Subramanian, V., Gurovich, D. & Lips, A. 2005 Wall slip and viscous dissipation in sheared foams: Effect of surface mobility. *Colloids Surf. A* **263**, 129–145.

Drenckhan, W., Cox, S. J., Delaney, G., Holste, H., Weaire, D. & Kern, N. 2005 Rheology of ordered foams—on the way to discrete microfluidics. *Colloids Surf. A* **263**, 52–64.

Hirasaki, G. J. & Lawson, J. B. 1985 Mechanisms of foam media: Apparent viscosity in smooth capillaries. *Soc. Pet. Eng. J.* **25**, 176–190.

Höhler, R. & Cohen-Addad, S. 2005 Rheology of liquid foams. *J. Phys. Condens. Matter* **17**, R1041–R1069.

Kornev, K. G., Neimark, A. V. & Rozhkov, A. N. 1999 Foam in porous media: thermodynamic and hydrodynamic peculiarities. *Adv. Colloid Interface Sci.* **82**, 127–187.

Marmottant, P. & Raven, J. P. 2009 Microfluidics with foams. *Soft Matter* **5**, 3385–3388.

Quéré, D. & de Ryck, A. 1998 Le mouillage dynamique des fibres. *Ann. Phys. Fr.* **23**, 1–149.

Raspet, R. & Griffiths, S. K. 1983 The reduction of blast noise with aqueous foams. *J. Acoust. Soc. Am.* **74**, 1757–1763.

Ratulowski, J. & Chang, H. C. 1990 Marangoni effects of trace impurities on the motion of long gas bubbles in capillaries. *J. Fluid Mech.* **210**, 303–328.

Raufaste, C., Foulon, A. & Dollet, B. 2009 Dissipation in quasi-two-dimensional flowing foams. *Phys. Fluids* **21**, 053102.

Rossen, W. R. & Gauglitz, P. A. 1990 Percolation theory of creation and mobilization of foams in porous media. *AIChE J.* **36**, 1176–1188.

Saugey, A., Drenckhan, W. & Weaire, D. 2006 Wall slip of bubbles in foams. *Phys. Fluids* **18**, 053101.

Shen, A. Q., Gleason, B., McKinley, G. H. & Stone, H. A. 2002 Fiber coating with surfactant solutions. *Phys. Fluids* **14**, 4055–4068.